

Non-linear oscillator models for the X-ray bursting of the microquasar GRS 1915+105

E. Massaro¹ • A. Ardito² • P. Ricciardi² •
F. Massa³ • T. Mineo⁴ • A. D'Ai⁵

Abstract The microquasar GRS 1915+105, exhibits a large variety of characteristic states, according to its luminosity, spectral state, and variability. The most interesting one is the so-called ρ -state, whose light curve shows recurrent bursts. This paper presents a model based on Fitzhugh-Nagumo equations containing two variables: x , linked to the source photon luminosity L detected by the MECS, and y related to the mean photon energy. We aim at providing a simple mathematical framework composed by non-linear differential equations useful to predict the observed light curve and the energy lags for the ρ -state and possibly other classes of the source. We studied the equilibrium state and the stability conditions of this system that includes one external parameter, J , that can be considered a function of the disk accretion rate. Our work is based on observations performed with the MECS on board *BeppoSAX* when the source was in ρ and ν mode, respectively. The evolution of the mean count rate and photon energy were derived from a study of the trajectories in the count rate - photon energy plane. Assuming J constant, we found a solution that reproduces

the x profile of the ρ class bursts and, unexpectedly, we found that y exhibited a time modulation similar to that of the mean energy. Moreover, assuming a slowly modulated J the solutions for x quite similar to those observed in the ν class light curves is reproduced. According these results, the outer mass accretion rate is probably responsible for the state transitions, but within the ρ -class it is constant. This finding makes stronger the heuristic meaning of the non-linear model and suggests a simple relation between the variable x and y . However, how a system of dynamical equations can be derived from the complex mathematical apparatus of accretion disks remains to be furtherly explored.

Keywords binaries - stars: individual: GRS 1915+105
- X-rays: stars - black hole physics - dynamical system

1 Introduction

It is known that phenomena occurring in accretion disks around black holes involve non-linear processes whose evolution can be described by a system of differential equations containing several quantities not directly observable. The only information we have concerns a fraction of the dissipated energy via electromagnetic radiation and usually observed in a rather limited frequency band. The stability of disk structures is also a very interesting subject of investigations since many years and theoretical analysis suggested that thermal and viscous instabilities can develop and establish a limit cycle behaviour.

To now the most important X-ray source exhibiting a complex variability, that on some occasions were characterized by long series of bursts as those expected by a limit cycle is the bright microquasar GRS 1915+105, discovered by Castro-Tirado et al. (1992). Only recently, Altamirano et al. (2011) reported the discovery

E. Massaro

Dipartimento di Fisica, Università La Sapienza, Piazzale A. Moro 2, I-00185 Roma, Italy

A. Ardito

P. Ricciardi

Dipartimento di Matematica, Università La Sapienza, Piazzale A. Moro 2, I-00185 Roma, Italy

F. Massa

INFN, Sezione Roma1, Università La Sapienza, Piazzale A. Moro 2, I-00185 Roma, Italy

T. Mineo

INAF, IASF Palermo, via U. La Malfa 153, I-90146 Palermo, Italy

A. D'Ai

Dipartimento di Fisica, Università di Palermo, Via Archirafi 36, I-90123 Palermo, Italy

of IGR J17091+3624 that exhibits variability patterns very similar to those of GRS 1915+105.

The large variety of light curves of GRS 1915+105, changing from quiescent states to fast series of short bursts and to much more complex patterns of alternating bursting and quiescent phases was classified in 12 types by Belloni et al. (2000) on the basis of a large collection of multi-epoch RXTE observations. New classes were added to these in the following years (Naik et al. 2002; Hannikainen et al. 2003, 2005) indicating that the source is potentially able to develop a rather large number of physical conditions from which more types of light curves can be originated. A description of such a complex phenomenology is given in the review paper by Fender and Belloni (2004).

From a general point of view the light curve variability classes of Belloni et al. (2000) can be grouped in three main types: *i*) light curves characterised only by small amplitude noisy fluctuations with respect to a stable average level (e.g. classes ϕ , χ , and δ); *ii*) light curves presenting series of (positive or negative) pulses (e.g. classes γ , κ , and ρ), occasionally exhibiting a rather stable recurrence time; *iii*) light curves structured in sequences of fast spikes alternating with rather quiescent and low brightness states (e.g. classes θ , λ , α , β and ν).

One of the most interesting variability classes is the ρ , lasting several days, whose light curves are quasi-regular series of bursts with a moderately variable recurrence time, usually in the range 40 – 100 seconds. The time and spectral properties of ρ class bursts have been investigated by several authors and the most recent papers on this subject are those by Neilsen et al. (2011, 2012) based on RXTE data and those by Massaro et al. (2010), Mineo et al. (2012), and Massa et al. (2013) who considered a long observation performed with *BeppoSAX* in October 2000. In particular, Massaro et al. (2010) reported that the mean recurrence time of the bursts increases with the source brightness, while Massa et al. (2013) investigated the properties of loops described by ρ bursts in a dynamical space where the coordinates are the count rate and the mean energy of photons. Since the first analysis (Taam et al. 1997) these recurrent bursts were associated with a limit cycle due to the onset of some disk instability. Several authors calculated possible theoretical light curves of the bolometric luminosity originating from disk instabilities. Complexity of hydrodynamic and thermodynamic equations does not allow a rather simple picture of the roles played by the involved physical quantities and the interpretation of data is not straightforward. Moreover, the limit cycle is often described in terms of disk quantities, such as the inte-

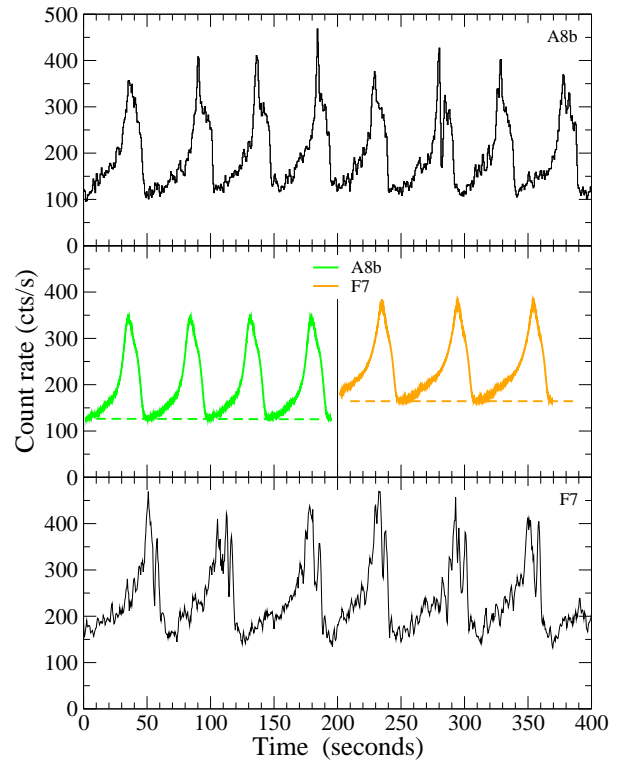


Fig. 1 Two 300 second long segments of the count rate of the MECS [1.4 – 10] keV for the data series A8b (top panel), F7 (bottom panel) of the long observation of October 2000 (see Massaro et al. 2010). A running average smoothing over 3 bins is applied to reduce the statistical Poissonian noise. The bin size of both series is 0.5 s. In the central panel two curves reproducing the mean bursts’ profile are shown: the green one on the left corresponds to the A8b data and the orange curve on the right to F7

grated density or the mass accretion rate, which are not directly observable

In the present paper we adopt a different approach and study the solutions of non-linear systems of two and three ordinary differential equations, whose solutions have very close similarities with the observational data series. These systems are mainly applied in the simulation of neuronal behaviour, and are able to describe quiescent, spiking and bursting activity like the one exhibited by GRS 1915+105. We will show that this approach makes possible to calculate light curves and phase space trajectories useful to investigate some dynamical aspects of the instability processes.

Non-linear oscillators were already considered in stellar physics for describing the convective energy transfer (Moore and Spiegel 1966) and the dynamics of pulsating variable stars (Regev and Buchler 1981; Buchler and Regev 1981; Buchler 1993). Non-linear

processes are also present in the coupling of the hot plasma and the radiation field in an accreting disk around a compact object. It is, therefore, likely that such equations can represent a useful mathematical approximation of much more complex relations in a suitable neighborhood of an equilibrium point. In this paper, we will not deal with the physical description of an accretion disk but will limit our study to show how the behaviour of GRS 1915+105 can be described by a unique oscillator and that some observed changes can be related to variations of a single parameter.

In Sect. 2 we describe the coarse structure of X-ray bursts and our method to compute the mean count rate and photon energy time curves. In Sect. 3 non-linear oscillator models are introduced and a solution with only two variables and constant parameters for the GRS 1915+105 data is presented; its equilibrium point and stability is studied in Sect. 4. In Sect. 5 we investigate the consequences of parameters' changes, and in Sect. 6 a possible extension to dynamical systems with three equations is presented. Finally, in Sect. 7 we discuss our results in the framework of current models for disk instabilities and limit cycles.

2 Time structure of ρ class bursts

We aim to demonstrate that the solutions of the equations of a rather simple non-linear oscillator are able to reproduce some of the main properties of the complex bursting patterns observed in GRS 1915+105. Considering that the most relevant information is mainly derived from the observed light curves it is useful to describe the structure of the bursts and to define typical time scale ratios. However, because of the variability of individual bursts, it is useful to use mean burst profiles for defining the main sections considered in our analysis. Mean pulse profiles and photon energy curves were obtained from a study of the trajectories in the count rate - mean photon energy ($CR-E$) plane. Fig. 1 shows two short segments of ρ class light curves (named A8b and F7, see Massaro et al. (2010), for the nomenclature and a description of the time properties of these data series) observed by the two operating MECS detectors on board the *BeppoSAX* satellite in October 2000. These curves are representative of the first and third of the three time intervals in which Massaro et al. (2010) divided the whole observation: in the first interval GRS 1915+105 exhibited a regular behaviour with only small changes of the burst recurrence time T_{rec} , the second interval showed an irregular behaviour, characterized by a peak multiplicity ≥ 3 , whereas in the third interval the source exhibited again a nearly regular variations with the mean count rate and the T_{rec} higher than in the first interval.

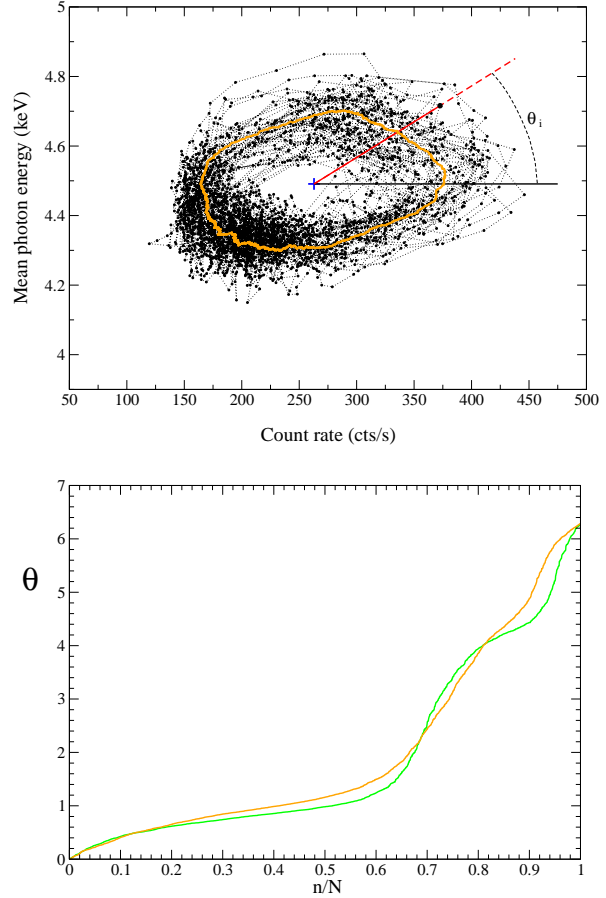


Fig. 2 Upper panel: Trajectory described by bursts of F7 series in the $CR-E$ space. The blue cross marks the centroid position. The red line is the segment connecting the centroid to a generic observed datum i (large dot) and the black line gives a direction from which the angle θ_i is measured. The orange line is the resulting mean loop. Lower panel: the plots of θ_n vs the ordering number n (normalized to the total number of data points in the series) for the A8b (green) and F7 (orange).

2.1 Mean burst profile reconstruction

In our method, the starting point for obtaining the mean CR and photon energy series is the analysis of loop trajectories described in the ($CR-E$) plane in the course of ρ class bursts. These trajectories were already described by Massa et al. (2013) and we refer to that paper for the details of the applied algorithms. The upper panel in Fig. 2 shows the loops of the F7 series and the central cross marks the centroid position computed through an iterative process.

Once known the centroid coordinates and the T_{rec} , obtained, for instance, by means of Fourier analysis, one considers a segment connecting the centroid with the i -th point of the data series; it is so possible to de-

fine a phase angle $0 < \theta_i < 2\pi$ with respect to a suitably chosen origin. Data are then ordered according to the values of θ and a new ordering index n is obtained for the series and a running average is applied to smooth fluctuations until a regular profile is obtained. The resulting plots of the ordered series θ_n vs n for the two considered series are given in the lower panel of Fig. 2. When time sampling index i increases the segment rotates in the plane with a variable angular velocity that can be obtained from differences of the phase angles between their consecutive values. The length of considered data series ensures that they contain many bursts and therefore the number of data points within any considered phase interval increases when the angular velocity is decreasing and viceversa. It is reasonable to assume a proportionality between the time necessary to cover the phase interval $\Delta t/T_{rec}$ and the fraction of data $\Delta n/N$ falling inside. One can thus compute the angular velocity of the vector as $(N/T_{rec})(\Delta\theta/\Delta n)$. Finally, one can simply transform the time scale to write two data sets where count rates and mean photon energies are functions of the resulting fraction of T_{rec} . The mean pulse profiles of series A8b and F7 are shown in the central panels of Fig. 1 and in Fig. 3, the corresponding mean loop in the $CR-E$ space is plotted in Fig. 2.

2.2 Burst structure

The observed structure of the ρ class bursts is rather complex and it is convenient to distinguish between a *coarse* and a *fine* time structure, the latter clearly apparent when a time binning lower than about 1 second is used. In particular the *Pulse* can contain two or more peaks of short duration, and in many cases the first is significantly higher than the others. This fine structure, however, appears noisy and, because of the high count rates in the *BeppoSAX* data, it can be partially affected by some instrumental effects as telemetry limitations. A good description of this fast and irregular phenomenon is quite difficult, whereas the mean profile enveloping these narrow peaks is rather stable. Therefore, in the following of the present work we will focus our study on the large scale structure.

According to Mineo et al. (2012), mean profiles, like those shown in Fig. 3, are divided into three main segments: the first is *Slow Leading Trail (SLT)* from the minimum level to half height, the second one is the *Pulse* whose typical duration is measured by its HWHM, followed by the *Fast Decaying Tail (FDT)*, in which the count rate decreases to its minimum. T_s that measures the duration of *SLT*, and T_p that corresponds to the *Pulse* length at the half height level, while the

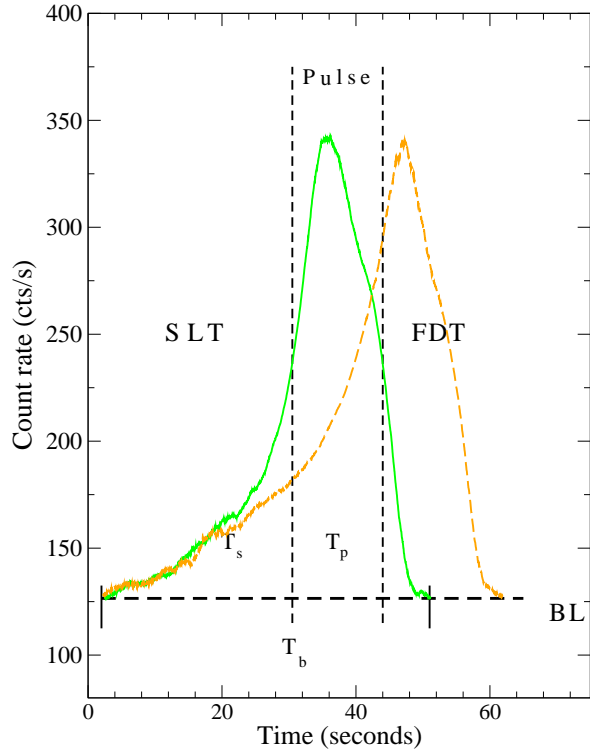


Fig. 3 Coarse time structure of bursts typical of the ρ . The green curve is the average profile of the A8b data series computed as explained in the text. The three main segments, *SLT*, *Pulse*, and *FDT* refer to the green curve. The total burst time is T_b , while the durations of *SLT* and *Pulse* are T_s and T_p , respectively. *BL* indicates the stable base-line level over which bursts are superposed. The dashed orange line is the mean pulse profile of the F7 data series translated to the same BL level of the other data for a better comparison of the differences in their profiles.

FDT duration is generally shorter than both these two covering a burst fraction of about 0.15 or less. T_b measures the total duration of individual bursts measured between two consecutive minima in the light curve. We can thus define the two ratios:

$$r_s = T_s / T_b \quad ; \quad r_p = T_p / T_b \quad (1)$$

characterizing the durations of *SLT* and *Pulse*, respectively. For example, for the mean A8b burst in Fig. 3 these ratios are $r_s = 0.58$ and $r_p = 0.28$, but we recall that they can vary up to several percents in individual bursts. In the case of the F7 mean burst, also plotted (orange curve) in Fig. 3 to show that the change in T_{rec} is due to an increase of the *SLT* duration, we have $r_s = 0.63$ and $r_p = 0.25$, while mean duration and height of the *Pulse* were practically unchanged.

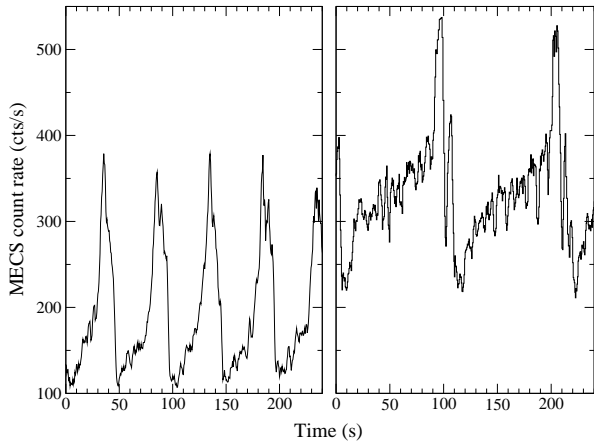


Fig. 4 Two short segments of MECS light curves illustrating changes of bursts' structure. Left panel: typical ρ class bursts from the A8b *BeppoSAX* data series of October 2000; right panel: bursts of a data series in the final part of the same observation when the variability class changed to ν . Note the large difference in the BL count rate and of the recurring time.

In Fig. 1 it is apparent an increase of the count rate occurred on time scales much longer than the typical T_{rec} : the lowest level is, in fact close to ~ 120 cts/s, as for the A8b series, while it increased to ~ 160 cts/s in F7. Moreover, the T_{rec} of bursts increased by about 30% (see Massaro et al. 2010, for details).

In addition to typical ρ class bursts other types are observed. For instance, relatively short sequences of bursts are present in other variability classes like α , β and ν (Belloni et al. 2000), but their structure can present different features as shown in the two panel of Fig. 4, where ρ and ν bursts are compared. The latter ones have a quite narrow and sharp spike instead of a structured *Pulse* and the leading trail is preceded by a fast initial increase just after a deep minimum. Note also that when ν bursts were observed the lowest count rate level was higher than that of the ρ class bursts by a factor of about 2.

When considering burst profiles in different energy ranges as [1.33.4] and [6.810.2] keV (see Fig. 2 in Massa et al. 2013) we found evidence of a few second delay of the higher energy count rate with respect to the lower energy one, and this delay increases using PDS data, above 15 keV. This Hard X-ray Delay (HXD) can be described by a change of the disk black body temperature during the burst from ~ 1 to ~ 2 keV in the SLT and *Pulse*, respectively (Fig. 11 in Massa et al. 2013). This temperature change corresponds to a variation of the mean energy of the photons observed by MECS, that although limited in a rather narrow range, is able to depict the HXD in the *CR-E* plane. The resulting

loop structure in this plane was used by Massa et al. (2013) to estimate the HXD. Furthermore, the results of the spectral analysis presented by Mineo et al. (2012) indicated that the HXD cannot be interpreted as the effect of photon scattering in a hot corona.

3 Dynamical equations of non-linear oscillators

The complex behaviour of GRS 1915+105 presents many similarities with that of a non-linear oscillating system as those used for describing signals in neuronal array. Mathematical aspects of this important subject were deeply investigated in the past half century and an extremely wide and technical literature is available. We apply these methods to the study of the X-ray signals observed from GRS 1915+105 and show that a rather simple, although non-linear, set of differential equations is able to reproduce the properties of some variability classes by adjusting only one parameter. This can pave the way to define a frame based on the same process useful to address theoretical models of disk oscillations and instabilities.

It is known from the theory of dynamical systems exhibiting either a quiescent or a spiking behaviour that they can be described by a system of first order non-linear differential equations. In many case, two equations can provide a satisfactory picture of a rather large class of phenomena, however, to take into account variation due to parameters changing over different time scales, usually much longer than those typical of the system, a third (or a fourth) variable must be introduced. A simple harmonic oscillator with a damping (or growing) term and subject to a constant forcing is described by two variables whose first time derivatives are linear functions of them.

More generally, considering three dynamical variables x , y and z , a rather general system having spiking and bursting solutions, thus involving changes on different time scales, can be written as:

$$\begin{aligned} \frac{dx}{dt} &= \frac{1}{A}[P_3(x) - b_1y - z] \\ \frac{dy}{dt} &= P_2(x) - b_2y \\ \frac{dz}{dt} &= \varepsilon[s(x - x_0) - z] \end{aligned} \quad (2)$$

where $P_2(x)$ and $P_3(x)$ are two polynomials of second and third degree, respectively:

$$\begin{aligned} P_3(x) &= -a_1x^3 + a_2x^2 + a_3x + a_4 \\ P_2(x) &= -a_5x^2 + a_6x + a_7 \end{aligned} \quad (3)$$

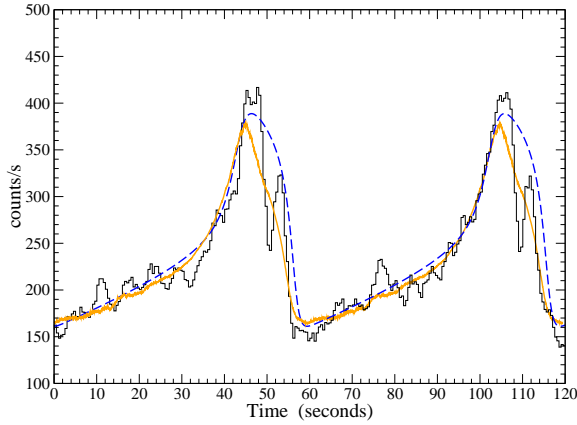


Fig. 5 A short segment of the F7 MECS light curve showing two bursts (black) with a time binning of 0.5 s. Data are smoothed with a running average over 5 bins. The orange curve is the mean reconstructed burst profile with the method described in the text. A solution of the FhN system, scaled and translated to match the data is plotted as the blue long-dashed line.

For particular values of the parameters, the system of Eq.(2) can be reduced to well studied differential equation systems. Thus for $a_2 = a_4 = a_5 = \varepsilon = 0$ we obtain the Fitzhugh-Nagumo (hereafter FhN) equations for only two variables, originally proposed by FitzHugh (1961), who named it as Bonhoeffer-Van der Pol oscillator, and extensively applied in simulating the behaviour of a neuron (e.g. Izhikevich 2007):

$$\begin{aligned}\frac{dx}{dt} &= \frac{1}{A}[-a_1x^3 + a_3x - b_1y] \\ \frac{dy}{dt} &= a_6x - b_2y + a_7\end{aligned}\quad (4)$$

For the choice of parameters, $A = 1, a_3 = a_6 = 0, b_1 = -1, b_2 = 1$, Eq.(2) gives the Hindmarsh-Rose (hereafter HR, Hindmarsh and Rose 1984) model (see also the tutorial paper by Shilnikov and Kolomiets 2008):

$$\begin{aligned}\frac{dx}{dt} &= -a_1x^3 + a_2x^2 + a_4 + y - z \\ \frac{dy}{dt} &= -a_5x^2 - y + a_7 \\ \frac{dz}{dt} &= \varepsilon[s(x - x_0) - z]\end{aligned}\quad (5)$$

An important characteristic of these equations is that non-linear terms imply that variables can evolve on different time scales. In the FhN model, for instance, x is the *fast* variable and y is *slow* one, whereas in the HR model z is slow and the two others are fast.

3.1 FhN model

To reproduce the stable bursting pattern of regular ρ class series, like the one observed in the A8b and F7 series (Fig. 1), it is convenient to change the variables to make simpler the FhN equations of Eq. (3) and to reduce the number of parameters. These algebraic manipulations are described in the Appendix I; the resulting equations are:

$$\begin{aligned}\frac{dx}{dt} &= -\rho x^3 + \chi x - \gamma y - J \\ \frac{dy}{dt} &= x - y\end{aligned}\quad (6)$$

where we indicated the two variables with x and y , as before, and the signs of the various terms were taken to have the parameters' values positive.

Parameters can be divided into *internal* and *external* ones if they appear or not as factors of the variables. We have thus only the external parameter J , whereas ρ, χ and γ are internal. Internal parameters are related to the physical state of the oscillating system, while the external one can be considered as a forcing of the system. In our first computations we will study the solutions obtained taking all the four parameters constant, although they, at least in principle, could change in time with the physical state of the source. To take into account their possible changes one or more further equations must be added to the above system to make it autonomous. Effects of possible variations of the parameters and, in particular those originating from slow changes of J will be discussed in Sect. 5.

Note also that the particular form of Eqs. (6) does not offer a simple interpretation for the physical meaning of the parameters. This fact depends on the adopted form and to the fact that we are interested in computing the time evolution of light curves. As shown in the Appendix II, the system in Eq.(6) can be written in a more general form, containing a quadratic term and an additional term to J , that leaves invariant the solutions for the two variables apart of a constant.

Numerical computations were performed by means of a Runge-Kutta fourth order integration routine (Press et al. 2007). Our first aim was to obtain a set of parameters' values for which the x variable gave a satisfactory solution for the F7 count rate light curve. Fig. 5 shows the resulting function compared with the mean burst profile (orange curve) and a short data segment. The agreement, although not exact, is fully satisfactory particularly for the *SLT* shape: we obtained that $r_s = 0.64$ and $r_p = 0.28$ quite close to those given in the previous Section for the F7 series. The adopted parameters' values were $\rho = 0.30, \chi = 33.0, \gamma = 222.0, J = 1100.0$.

We remark here that these values were not obtained by means of a best fit optimization procedure, very hard to apply to the equation system solutions because of their high variability also for small changes of parameters. Note that the model does not describe substructures in the *Pulse*, and that it is broader than observed close to the maximum; however, the *FDT* appears sharp as in the data. In the following we will refer to this solution as ‘FhN-A’ model.

A very important and unexpected finding of this solution is that the variable y reproduces well the evolution of mean photon energy, or disk temperature (Massa et al. 2013). The comparison between the mean burst and energy profiles with the x and y curves is shown in the top and central panels of Fig. 6. Data and model curves were normalized, after subtraction of their central values, so to have comparable amplitudes. In the bottom panel of Fig. 6 we plotted the time derivatives of the two computed series to show more clearly how their changes occur on different time scales: the y derivative (magenta curve) is always limited in a rather small interval, whereas that of x remains small and positive during the *SLT*, dropping to a high negative value in the fast decaying phase of the *Pulse* and *FDT*. One can also note a time delay between the two curves in the same direction of that in the observed data (Massa et al. 2013), although the latter resulted on the average smaller by about 25%.

This finding makes stronger the heuristic meaning of the non-linear model and suggests a simple linear relation between the variable x with the source photon luminosity (i.e. the rate of X-ray emitted photons) L detected in the MECS energy range, or any other physical quantity proportional to it as the photon density in the emitting regions of the disk, and of y with the mean energy of photons or the mean disk temperature, otherwise the main features of both data series would not be so finely matched.

$$\begin{aligned} x(t) &= C_L[L(t) - L_0] \\ y(t) &= C_E[E(t) - E_0] \end{aligned} \quad (7)$$

where L_0 and E_0 are two constant values of the photon luminosity and mean photon energy, respectively, C_L and C_E are two dimensional coefficients useful for writing our equations in a non-dimensional form. The correspondence between the formal variables x , y and the physical observable quantities, is also apparent from the x, y plot (hereafter phase space plot) that results similar, except for the scale factors, to the count-rate vs mean energy plot studied by Massa et al. (2013) (see also Fig.14 in Janiuk and Czerny 2005). This is clearly shown in Fig. 7, where the loop of the stable cycle described by Eqs.(6) is reported.

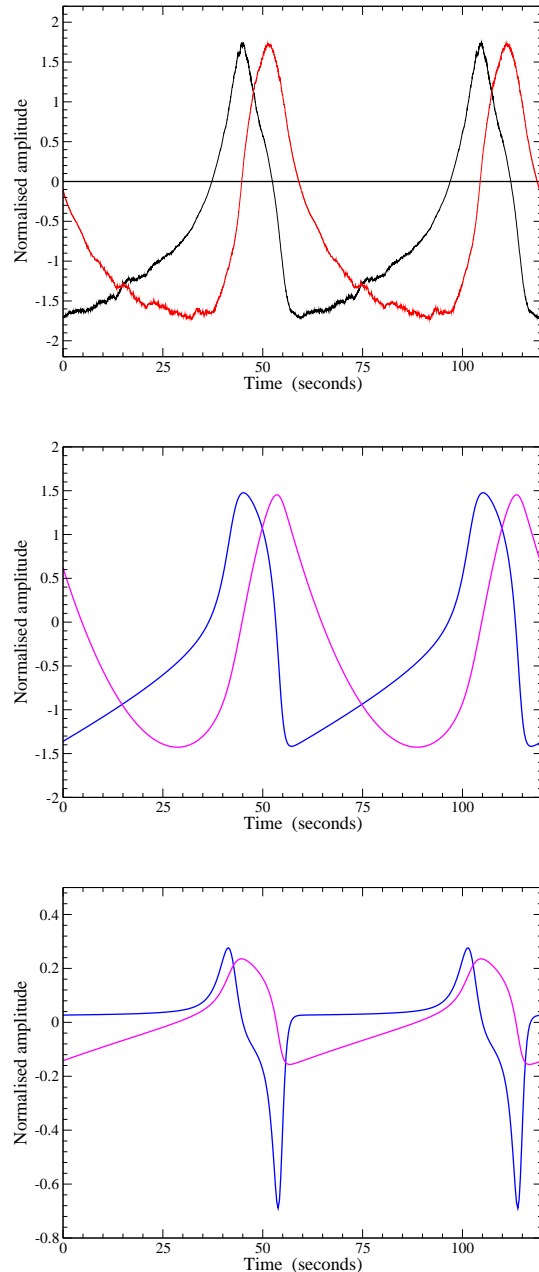


Fig. 6 Top panel: time evolution of the mean pulse profile (black) and mean photon energy (red) of the F7 series; Central panel: results obtained from the model FhN-A with the same parameters as in Fig. 5, blue and magenta lines represent the time behaviour of the x and y variables, respectively using the same time scale of the upper panel, Bottom panel: time derivatives of the x and y series shown in the central panel plotted using the same colors.

4 Equilibrium points and stability

The study of equilibrium points is important for understanding which are the conditions to develop a limit

cycle behaviour (see, for instance Hale and Kocak 1991; Farkas 1994; Strogatz 1994). Equilibrium points are obtained from the solutions of the system for $(dx/dt) = (dy/dt) = 0$, that for Eqs.(6) reads:

$$\begin{aligned}\gamma y &= -\rho x^3 + \chi x - J \\ x &= y\end{aligned}\quad (8)$$

that can be easily reduced to the cubic equation:

$$\varphi(x) = x^3 + \frac{\gamma - \chi}{\rho} x + \frac{J}{\rho} = 0 \quad (9)$$

Light curves presented in Figs. 5 and 6 (FhN-A model) were obtained for $\chi/\gamma = 33/222 < 1$, and therefore the case of interest is the one with a unique (negative) equilibrium point, (see Appendix III), whose value for the considered parameters is $x_* = y_* = -5.54891$. In the x, y plane this equilibrium point is at the intersect between the $x = y$ line with the cubic curve $(dx/dt) = -\rho x^3 + \chi x - J$ (these lines are named *nullclines*) which are plotted in red in Fig. 7. Note that for about all the *SLT*, in which the dynamical behaviour is ruled by the slow variable y , the trajectory remains very close to the x nullcline, and only after it approaches the other nullcline near the equilibrium point, the fast variable turns to be dominant. The trajectory rapidly moves to the right to reach the x maximum on the other branch of the cubic line and then it decreases in a very short time towards the minimum on the former branch.

The results of the stability analysis of solutions in a neighborhood of this equilibrium point are given in the Appendix III. The most interesting result is that around this equilibrium point a limit cycle can be established.

The equilibrium point corresponding to the parameters' values of the FhN-A model is quite close to the stability boundary and a relatively small change of only one of these values can move the state outside this region, and as a consequence the limit cycle disappears. For example, keeping χ and ρ fixed at the above values, the stability is reached when $|x_*| > \sqrt{(\chi - 1)/3\rho} = 5.9628$, rather close to the equilibrium value. We will show in the next Section how the changes of the parameters affect the solution and whether these modifications can account for the observed variability of GRS 1915+105.

5 Effects of variations of parameters' values

One can use the numerical integration code to investigate how the burst shape and the recurrence time change with the parameters' values in Eqs.(6). It is not

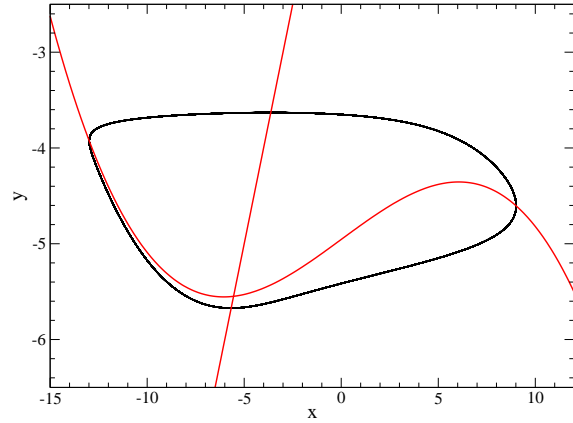


Fig. 7 Phase space plot of the periodic solution of Eqs.(6) computed using the same parameters' values of Fig. 5. The loop is described in anti-clockwise direction as observed in the count-rate vs mean energy plots discussed by Massa et al. (2013). Red lines are the *nullclines* for the model FhN-A.

simple to disentangle the role of individual parameters because they are all combined together in determining the *nullclines* and the equilibrium point. Therefore, in the following we will present the effects due to the change of only one of the parameters with the other three kept frozen to those of the model FhN-A.

The four panels in Fig. 8 summarize these results: they illustrate how a change of only one parameter can affect the light curve pattern. All the scales of the various panel are the same to make easy the comparison of the signals' profiles. In each panel, the third curve from the top is the one of model FhN-A that we plotted to make easy the comparison. A common characteristics is well evident: for all parameters there is a critical value for which the position of the equilibrium moves into a stability region and the signal amplitudes decrease to a steady level. These critical values are close to 0.34, 29.5, 210, and 1190 for ρ , χ , γ and J respectively. In all these cases, they are remarkably close to the values found for the F7 series, indicating that during this time series, the system was close to switch-off the oscillations relaxing into a quasi-steady state. Note also that variations of all the parameters can modify the burts recurrence time.

5.1 ρ changes

Changes of the signal due to a variation of ρ are shown in the let upper panel of Fig. 8. A rather small increase of ρ from 0.30 to about 0.34 produces a switch off of the bursting and a stable level close to the mean value is

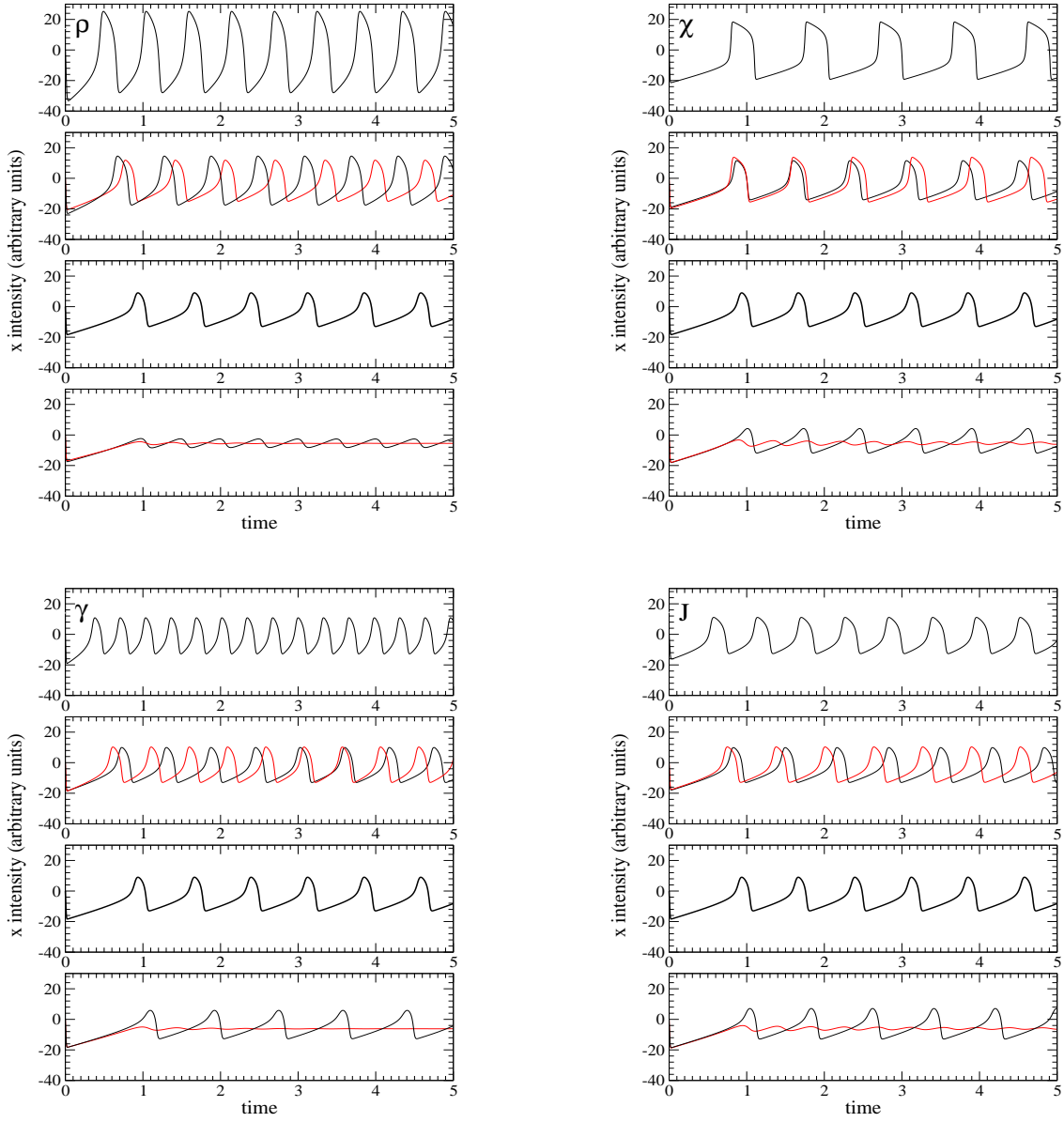


Fig. 8 Variation of the burst period and amplitude for different values of the parameter ρ . Top to bottom: 0.06, 0.16 (black) and 0.22 (red), 0.30, 0.34 (black) and 0.38 (red). Variation of the burst period and amplitude for different values of the parameter χ . Top to bottom: 80.0, 60.0 (red) and 40.0 (black), 33.0, 30.0 (black) and 20.0 (red). Variation of the burst period and amplitude for different values of the parameter γ . Top to bottom: 500, 300 (red) and 260 (black), 222, 212 (black) and 200 (red). Variation of the burst period and amplitude for different values of the parameter J . Top to bottom: 600, 900 (red) and 1000 (black), 1100, 1150 (black) and 1200 (red).

maintained. Stable burst patterns are obtained for decreasing ρ down to quite small values around 0.05. All the resulting curves show that a decrease of the T_{rec} is associated with an increase of the amplitude. Modifications of the recurrence time produce also a shortening of the *SLT* and an increase of the *Pulse* width with the consequence that the curve profile becomes more symmetric, with $r_s \approx r_p \approx 0.5$.

5.2 χ changes

The right upper panel of Fig. 8 shows that a decrease of χ from 33.0 to about 30.0 is sufficient to reduce the burst amplitude by a factor of ~ 2 , and a further decrease will produce the almost disappearance of bursts with constant level remarkably close to the previous one. An increase of χ produces an increase of T_{rec} that

appears mainly due to a broadening of the *Pulse* width instead of the *SLT*.

5.3 γ changes

At variance with the two previous parameters, changes of γ do not appear to affect significantly the burst amplitude but produce large variations of the burst recurrence time. In the left lower panel of Fig. 8 one can see that the *Pulse* duration is practically unaffected by these changes, which affect mainly the length of the *SLT*. This result agrees very well with the observed differences between A8b and F7 series. Again we found that a relatively small decrease of χ , from 222 to values lower than ~ 210 , would relax the bursting to a stable level, very close to those found above.

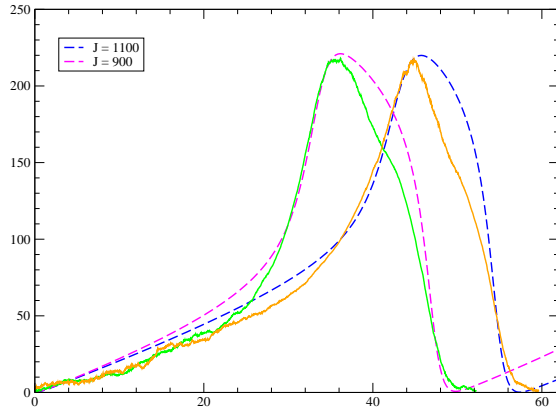


Fig. 9 Comparison between the reconstructed pulse profiles of series F7 (orange) and A8b (green) with the results of the FhN-A model for $J=1100$ (blue dashed line) and 900 (magenta dashed line). Time scaling is the same for the two computed series.

5.4 J changes

Effects of J changes are interesting because this is the only external parameter of the model. Results are given in the right lower panel in Fig. 8: the *Pulse* width is practically unaffected by these changes whereas T_{rec} appears to be much more variable, because of different durations of the *SLT*. For low values of J the curve profile tends to be symmetric, with a short *SLT* and the corresponding values of r_s and r_p approach to 0.5. The typical ρ burst profile begins to be clearly recognizable for $J > 500$, and approaches the observed one when J is higher than 800. The critical value of J for the burst quenching is close to 1190.

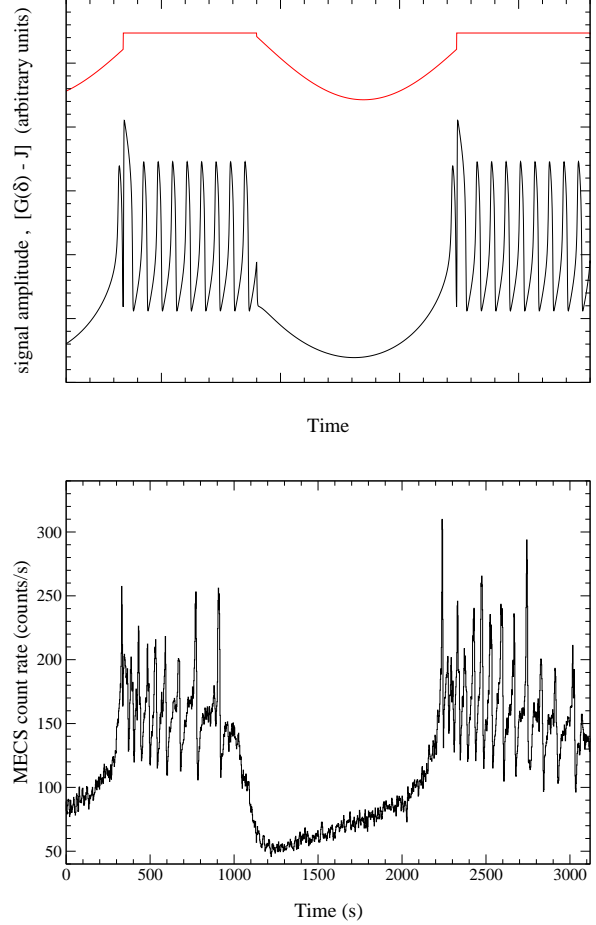


Fig. 10 Upper panel: computed light curve (black line) when the $[G(\delta) - J]$ term changes as represented by the red line. Units are arbitrary. Lower panel: GRS 1915+105 light curve in the ν class observed by MECS2 detector on 1996 November 11.

According to these results the main features of A8b series must correspond to a lower J . We found that a J value around 900 gives a pulse profile and T_{rec} in a satisfactory agreement with that of A8b series when the same scale factors of F7 data are used. The shape of the *Pulse*, however, is slightly different from the observed one, being this narrower than the one computed by the model. A comparison between these results and the mean profiles is shown in Fig. 9.

5.5 Slow changes of J

It is very interesting to show how a nearly regular modulation of J on time scales longer than the typical recurrence time of bursts can produce different types of light curves resembling very much those of other GRS 1915+105 variability classes. For instance, the upper panel of Fig. 10 shows what happens when J has a

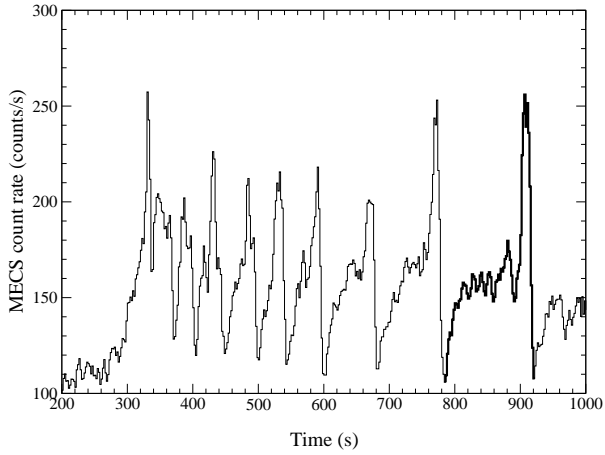


Fig. 11 Detail of the MECS2 light curve of GRS 1915+105 shown in the lower panel of Fig. 10. The thick plotted burst is the same shown in Fig. 12.

slow modulation like that in the upper red curve. Numerical calculations were performed by shifting both variables of $\delta = 24.0$ (see Appendix II) to maintain always positive the forcing term $[G(\delta) - J]$. The resulting light curve presents an alternance of bright states with a burst sequence superposed and low brightness states, remarkably similar to those characterizing the ν class of (Belloni et al. 2000), as apparent from the light curve in the lower panel from a *BeppoSAX* observation of GRS 1915+105 performed on 1996 November 11.

Note, in particular, that in addition to the main modulation other features agree with observations, e.g. the first spikes reach higher count rates with respect to the following ones. More realistic light curves are obtained including random fluctuations of J , as could be expected in a turbulent disk, that simulate either the observed noise and the small changes of T_{rec} .

A spectral analysis of RXTE observations of GRS 1915+105 in the β class was described by Migliari & Belloni (2003) who reached the conclusion that the mass accretion rate is variable with its highest value at the minimum brightness. Results in Fig. 10 show that the J must have a different behaviour with a stable high value during the spikes' series followed by a slowly variable having a minimum practically simultaneous with the lowest brightness level.

Variations of J on time scales of the order a burst duration (typically ~ 100 s) can explain burst profiles as those of ν class (Fig. 4). Fig. 11 shows a detail of the first burst series in Fig. 10, where nine events are clearly apparent. Their duration increases more than a factor of 3, from ~ 40 s to ~ 140 s of the last one and the shape of some events has an initial well defined minimum followed by a fast increase turning

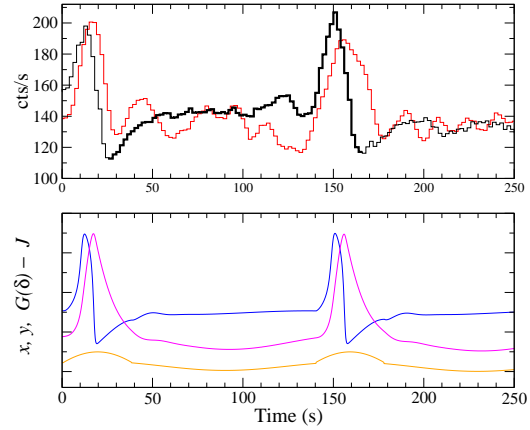


Fig. 12 Upper panel: MECS2 light curve of a burst of the observation on 1996 November 11 (black), red line is the corresponding mean photon energy scaled to the mean count rate level. Bin width is 2 seconds, all data have been smoothed with a running average over 5 bins to reduce the statistical noise. Thick line data are used to help the correspondence with data in Fig. 11. Lower panel: model light curve of the x variable (blue line) obtained from the FhN-A model assuming a modulated $G(\delta) - J$ according to the orange curve. The magenta line describes the variation of y variable. Time scale and amplitudes of these curves were scaled to match the data in the upper panel.

in a rather flat shoulder which ends in a sharp spike (Fig. 12 upper panel). This pattern is obtained for the x variable in FhN-A model (Fig. 12 lower panel) assuming that J has modulation as that shown by orange line. In the same panel we reported also the solution for the y (magenta curve) which corresponds well to the mean photon energy. The other three model parameters are unchanged demonstrating that the variation of only one quantity is able to reproduce all these behaviours.

An important point is that J values producing the solution in Fig. 12 vary in the range $[1225, 1390]$ with a mean value of 1330. These values are higher than the one used to reproduce the ρ class data and move the system into the locally stable region (see Appendix III, B region in Fig. A1). Thus no limit cycle can exist and the photon luminosity changes must be originated from J variations. However, according to our model, it is not necessary that J must have a modulation amplitude comparable to that of the photon luminosity: a relatively small change can, in fact, produce much higher brightness changes because of the occurrence of non-linear effects.

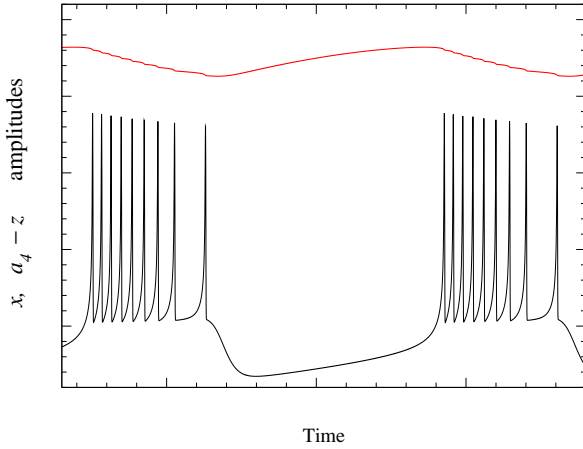


Fig. 13 Light curves (x black line, $a_4 - z$ red line) computed by means of the HR model for reproducing the one observed by *BeppoSAX* and reported in the lower panel of Fig. 10. Units are arbitrary.

6 Results from the Hindmarsh-Rose model

In the FhN model time variations of a parameter must be taken as an input function and consequently the system is not autonomous. This difficulty can be solved by introducing a third variable, whose variations have a time scale much longer than those of x and y , as in the case of the system proposed by Hindmarsh and Rose (1984, see Eq.(5) in Sec. 4). We omit here the mathematical properties of the equations, and refer the reader to the above cited specific papers, and limit ourselves to present an interesting result obtained from numerical integration of Eqs. (5). FhN-A results, of course, are easily obtained by HR model by taking $\varepsilon = 0$ and thus reducing the system only to two equations, but much more interesting are the solutions when three equations are used. In Eqs. (5) z is the slow variable and plays a role similar to that of $J(t)$ in the previous Section, while x and y are the fast ones. A possible light curve (x variable) is shown in Fig. 10, computed with the following values of the parameters: $\varepsilon = 0.001$, $a_1 = 1.0$, $a_2 = 3.0$, $a_4 = 1.9$, $a_5 = 5.0$, $a_7 = -1.0$, $s = 4.0$ and $x_0 = -1.1$. In the same figure it is also plotted the corresponding curve of the slow $a_4 - z$ variable (red line) which shows that it varies on the same scale of burst sequence, but not on that of individual spikes. The similarity with the observed data in the lower panel of Fig. 10 is impressive: in particular, non bursting phases exhibit very similar trends and also there is the very interesting property that the recurrence time of spikes during the bursting phase increases approaching the end of the series. It is remarkable to mention that the same curve was early obtained by Hindmarsh & Rose (1984) for reproducing the behaviour of neurons.

It is interesting to mention how the solution changes with the value of ε : when it decreases the length of burst sequence increases until it evolves in a long and regular series of repeating spikes, while for increasing ε the spike number decreases to unity giving again a regular series of spikes, but for values higher than 0.0402 the solution changes and approaches rapidly a stable state.

7 Discussion

It is well known that the X-ray source GRS 1915+105, the prototype of microquasars, exhibits a large number of variability classes changing from quasi-quiet states to long and regular series of bursts, persisting for several days, and irregular variations on different time scales. Many theoretical computations, generally based only on radial disk model equations, i.e. integrated over the thickness, and assuming the α prescription (Shakura and Sunyaev 1976) for the gas viscosity, have been performed in the past years since the early work by Taam et al. (1997), with the goal of modelling these puzzling light curves.

We followed a different approach and tried to reproduce some variability patterns of GRS 1915+105 by means of non-linear systems of differential equations, which have been extensively investigated in the literature in the context of neuronal activity to explain quiescent, bursting and spiking states. Several systems of equations have been proposed, since the original work by Hodgkin and Huxley (1952). We have shown that one of the simplest systems for neuronal model, developed by FitzHugh (1961) from the Banhooffer-van der Pol oscillator and electronically realized by Nagumo et al. (1962), consisting only of two differential equations with a single non-linear term, is able to reproduce some features of the ρ variability class of GRS 1915+105. We wrote the system in a form containing only four parameters and studied its equilibrium state and the stability conditions for which is possible to obtain a limit cycle.

In the following paragraphs we first summarize our results and then discuss a possible interpretation in comparison with some proposed instability mechanisms.

7.1 Summary of main results

FitzHugh-Nagumo equations contain four parameters, three of which, ρ , χ and γ , relate the x and y time derivatives to the variables and are named internal, while the only external parameter J can play the same

role of a forcing. We adjusted parameters' values to obtain a solution for x reproducing the gross profile of the ρ class bursts and, unexpectedly, we found that the other variable y exhibited a time modulation remarkably similar to that of the mean energy (or the temperature) of photons as found by Massa et al. (2013) (FhN-A model). We underline that changes of x and y occur on two different time scales, fast and slow, respectively. This result is obtained with a constant J value and therefore it implies that this bursting is intrinsic to the non-linear oscillations and do not require an external modulation, as in the well known self-oscillation phenomenon (see for instance the recent review paper by Jenkins (2013)). Moreover, the the delay of the emission at high energy with respect to the low energy one, as resulting from the plots in Fig. 6, is a direct consequence of the physical mechanism responsible for the bursting and other mechanisms as photon scattering from a hot corona are not necessary, in agreement with the results of spectral analysis (Mineo et al. 2012). All these results agree remarkably well with the delay measurements reported by Massa et al. (2013) and with the evolution of the disk and corona photon luminosity along the burst obtained with the spectral analysis presented by Mineo et al. (2012). The FhN-A model, therefore, appears to have a relevant heuristic value and should not be simply considered an ad-hoc mathematical description of the observed data.

It is also interesting to note that the non linearity of the FhN equations implies that the burst recurrence time is also depending upon the external parameter J . The lower right panel in Fig. 8 shows that changes of T_{rec} are mainly due to a modification of the SLT length. From the curves in Fig. 9, we see that the change of T_{rec} from A8b to F7 data series can be accounted for an increase of J by about 20%, comparable to that of BL level in Fig. 1. This finding suggests that this parameter can be likely related to an external mass-accretion rate (\dot{m} at large radii) that is the main regulator of the disk photon luminosity. Slow variations of this quantity and the consequent changes of $J(\dot{m})$ can thus move the oscillator across the boundary between the stability or instability region, and *vice versa* (see Appendix III) with a consequent appearance or disappearance of a bursting limit cycle. Effects of \dot{m} changes may also be responsible of some of the variability classes as those classified by Belloni et al. (2000). In Sect. 5.5 we found that a high and slowly modulated J can produce solutions for x with an alternance of spikes and quasi quiescent states quite similar to those observed in the ν class light curves.

Under this respect, it appears more interesting the result obtained from the HR model, which includes

one more variable and a corresponding equation. The bursting solution in Fig. 13 presents such a striking similarity with the data, such as the increasing recurrence time of bursts or the shape of the quiescent part (see lower panel in Fig. 10), that appears very unlikely that it is only a chance result. Our solution is essentially of the same type of those discussed by Shilnikov and Kolomiets (2008) and the mathematical properties are extensively presented in that paper.

We can conclude that the apparent complex behaviour of GRS 1915+105 seems to be mainly regulated by a single non-linear oscillator driven by a unique parameter, whose changes are responsible at least for some of variability classes. The non-linear oscillator model implies that there is an interplay between the two (or three) variables and therefore some caveats must be considered in the interpretation of spectral parameters' values derived by spectral fitting of the data, such as the widely used *diskbb* (Mitsuda et al. 1984) or others in XSPEC. For instance, changes of the disk inner radius may alternatively be considered as a luminosity normalization rather than an evidence of a real change in the disk radial extension.

It is unclear whether the models described in the present paper are the most appropriate ones for GRS 1915+105 or if other variables or terms must be introduced in the differential equations. It is an open problem how a system of dynamical equations can be derived from the complex mathematical apparatus of accretion disks and this requires new deep theoretical investigations.

Useful indications in this direction, however, can be retrieved from some interesting previously published works.

7.2 Disk instabilities and the ρ class limit cycle

Studies of the development of instabilities in accretion disks started several decades ago (e.g. Lightman and Eardley 1974; Pringle et al. 1973; Shakura and Sunyaev 1976) and up to now originated an extensive literature. Taam and Lin (1984), in particular, computed by means of numerical integration of the non-linear disk equations to investigate thermal-viscous instabilities and obtained a few theoretical light curves having recurrent bursts consisting by a slow rising portion followed by a very narrow and high peak, more similar to those in the right panel of Fig. 4 or in Fig. 12, rather than to those in Fig. 5. With the discovery of the ρ class variability in GRS 1915+105, Taam et al. (1997) investigated the time and spectral properties of the bursts and proposed an interpretation based on the instability discussed in the previous paper. However, these authors invoked for explaining the delayed hard emission

a reflection in the frame of a disk-corona model. Later Nayakshin et al. (2000) to reproduce some classes of light curves of GRS 1915+105 proposed a disk model with a rapidly variable viscosity and an upper limit to the energy fraction transferred to the disk emission. Watarai and Mineshige (2003) studied a model with a modified version of the α -viscosity prescription law with respect to the standard one and introduced a power law dependence of viscosity stress tensor $\mathcal{T}_{r\varphi}$ on the ratio between the gas p_{gas} and the total pressure $\beta = p_{gas}/(p_{gas} + p_{rad})$:

$$\mathcal{T}_{r\varphi} = -\alpha_0 \beta^\mu \Pi \quad (10)$$

where Π is the height integrated pressure.

The resulting light curves exhibit the typical bursting behaviour and the variable recurrence time results from changes of the exponent μ . In these models, however, there is no delay between temperature and photon luminosity as observed in the ρ class bursts (Massa et al. 2013).

A further investigation of the limit cycle light curves was performed by Merloni and Nayakshin (2006) who considered a magnetized disk in which magnetic turbulent stresses inside the disk scale with the pressure as ($0 < \mu < 2$):

$$\mathcal{T}_{r\varphi} = -\alpha_0 p_{tot}^{1-\mu/2} p_{gas}^{\mu/2} \quad (11)$$

Their calculated light curves for an accreting black hole of $10 M_\odot$ and $\mu = 0.1$ have a recurrence time of bursts increasing with the mass accretion rate, in a qualitative agreement with our results. Unfortunately, the simultaneous temperature evolution is not given and a full comparison with the data and the results of the FhN-A model is not possible. However, the approach of an energy transfer instability in a magnetized disk appears one of the most promising for the understanding of physical processes regulating the instability.

A model for the ρ class has been recently proposed by Neilsen et al. (2012, 2011) who interpreted the bursting as a consequence of a similar modulation in the mass accretion rate. In these works, authors used RXTE/PCA and Chandra/HETGS data to characterize the spectral modifications according to the burst phase. A model of soft thermal disk component and hard Comptonized emission shows that changes in the parameters are smooth for most of the burst phases, but a significant spectral modification is observed during the pulse. At this phase it is observed a strong decrease of the inner disk radius (up to $\sim 2 R_g$, that would require a spinning black-hole with an adimensional angular momentum per unit mass $a \simeq 0.9$ if this minimal radius is identified with that of the last stable orbit), and a

strong increase in the coronal electron opacity (where most of the disk emission is Thomson scattered). Some authors (e.g. Artemova et al. 1996) have therefore argued that during the pulse a recurrent set of steps are operating: when at small disk radii, local Eddington limit is reached, a radiation pressure instability develops and, consequently, part of the inner disk is vaporized into an optically thick, completely ionized, cloud. This cloud emits also part of its energy as thermal bremsstrahlung emission (hard pulse). Modification of this primary radiation causes also changes at large outer disk radii, as it strongly modified the structure of any (thermally/radiation driven) disk wind. Because the fraction of the mass outflow that is dispersed into a wind (which if channelled by the disk magnetic field lines may become a jet) modifies the fraction of the accretion mass rate, this leads to generation of mass density waves that propagate toward the accretor, giving rise to the burst typical recurrent pattern. Such scenario appears to be consistent with a combination of spectroscopic detailed line diagnostic and broadband coverage of the spectral shape. However, our approach shows that the limit-cycle behaviour can also be understood independently from any fitted spectral decomposition. If the strong relation of the global mass accretion rate with J holds, the link between the outflow rate with the inner mass accretion rate could not be strictly required.

We have shown that the outer mass accretion rate is probably responsible for passages between one state to another, but within the ρ -class state, J is constant, and the oscillating mechanism is still at work. This does not mean that changes at small radii should not impact the wind physical properties, but only that the claimed strong feed-back of the two zones may not be necessary for the development of the limit-cycle instability. We note that a detailed modelling of the expected changes in the energy spectra would require a translation of the differential equations into the proper physical radiation components, which would lead beyond the aims of the present work.

Acknowledgements The authors are grateful to Marco Salvati and Andrea Tramacere for very useful discussion and comments. The CNR Institutes and the *BeppoSAX* Science Data Center are financially supported by the Italian Space Agency (ASI) in the framework of the *BeppoSAX* mission.

References

- Altamirano, D., Belloni, T., Linares, M., van der Klis, M., Wijnands, R., Curran, P.A., Kalamkar, M., Stiele, H., Motta, S., Muñoz-Darias, T., Casella, P., Krimm, H.: *Astrophys. J. Lett.* **742**, 17 (2011). 1112.2393. doi:10.1088/2041-8205/742/2/L17
- Artemova, I.V., Bisnovatyi-Kogan, G.S., Bjoernsson, G., Novikov, I.D.: *Astrophys. J.* **456**, 119 (1996).
- Belloni, T., Klein-Wolt, M., Méndez, M., van der Klis, M., van Paradijs, J.: *A&A* **355**, 271 (2000)
- Buchler, J.R.: *Astrophys. Space Sci.* **210**, 9 (1993). doi:10.1007/BF00657870
- Buchler, J.R., Regev, O.: *Astrophys. J.* **250**, 776 (1981). doi:10.1086/159427
- Castro-Tirado, A.J., Brandt, S., Lund, N.: *IAUC* **5590**, 2 (1992)
- Farkas, M.: *Periodic Motions*. Springer, New York, NY, USA (1994)
- Fender, R., Belloni, T.: *Annu. Rev. Astron. Astrophys.* **42**, 317 (2004). doi:10.1146/annurev.astro.42.053102.134031
- FitzHugh, R.: *Biophys. J* **1**, 445 (1961)
- Hale, J.K., Kocak, H.: *Dynamics and Bifurcations*. Springer, New York, NY, USA (1991)
- Hannikainen, D.C., Vilhu, O., Rodriguez, J., Brandt, S., Westergaard, N.J., Lund, N., Mocœur, I., Durouchoux, P., Belloni, T., Castro-Tirado, A., Charles, P.A., Dean, A.J., Fender, R.P., Feroci, M., Hakala, P., Hunstead, R.W., Kaiser, C.R., King, A., Mirabel, I.F., Pooley, G.G., Poutanen, J., Wu, K., Zdziarski, A.A.: *Astron. Astrophys.* **411**, 415 (2003). arXiv:astro-ph/0309532. doi:10.1051/0004-6361:20031444
- Hannikainen, D.C., Rodriguez, J., Vilhu, O., Hjalmarsson, L., Zdziarski, A.A., Belloni, T., Poutanen, J., Wu, K., Shaw, S.E., Beckmann, V., Hunstead, R.W., Pooley, G.G., Westergaard, N.J., Mirabel, I.F., Hakala, P., Castro-Tirado, A., Durouchoux, P.: *Astron. Astrophys.* **435**, 995 (2005). arXiv:astro-ph/0502438. doi:10.1051/0004-6361:20042250
- Hindmarsh, J.L., Rose, R.M.: *Proc. R. Soc. London, Ser. B* **221**, 87 (1984)
- Hodgkin, A.L., Huxley, A.F.: *The Journal of Physiology* (1952)
- Izhikevich, E.: *The MIT Press*, Cambridge, MA, 111 (2007)
- Janiuk, A., Czerny, B.: *Mon. Not. R. Astron. Soc.* **356**, 205 (2005). arXiv:astro-ph/0409671. doi:10.1111/j.1365-2966.2004.08435.x
- Jenkins, A.: *Physics Reports* **525**(2), 167 (2013). doi:10.1016/j.physrep.2012.10.007
- Lightman, A.P., Eardley, D.M.: *Astrophys. J. Lett.* **187**, 1 (1974). doi:10.1086/181377
- Massa, F., Massaro, E., Mineo, T., D’Ai, A., Feroci, M., Casella, P., Belloni, T.: *Astron. Astrophys.* **556**, 84 (2013). 1306.1628. doi:10.1051/0004-6361/201220651
- Massaro, E., Ventura, G., Massa, F., Feroci, M., Mineo, T., Cusumano, G., Casella, P., Belloni, T.: *Astron. Astrophys.* **513**, 21 (2010). 1001.4406. doi:10.1051/0004-6361/200912908
- Merloni, A., Nayakshin, S.: *Mon. Not. R. Astron. Soc.* **372**, 728 (2006). astro-ph/0603159. doi:10.1111/j.1365-2966.2006.10889.x
- Migliari, S., Belloni, T.: *Astron. Astrophys.* **404**, 283 (2003). astro-ph/0303664. doi:10.1051/0004-6361:20030484
- Mineo, T., Massaro, E., D’Ai, A., Massa, F., Feroci, M., Ventura, G., Casella, P., Ferrigno, C., Belloni, T.: *Astron. Astrophys.* **537**, 18 (2012). 1110.5199. doi:10.1051/0004-6361/201117369
- Mitsuda, K., Inoue, H., Koyama, K., Makishima, K., Matsuoka, M., Ogawara, Y., Suzuki, K., Tanaka, Y., Shibazaki, N., Hirano, T.: *Publ. Astron. Soc. Jpn.* **36**, 741 (1984)
- Moore, D.W., Spiegel, E.A.: *Astrophys. J.* **143**, 871 (1966). doi:10.1086/148562
- Nagumo, J., Arimoto, S., Yoshizawa, S.: *Proceedings of the IRE* **50**(10), 2061 (1962). doi:10.1109/jrproc.1962.288235
- Naik, S., Rao, A.R., Chakrabarti, S.K.: *Journal of Astrophysics and Astronomy* **23**, 213 (2002). astro-ph/0211515. doi:10.1007/BF02702284
- Nayakshin, S., Rappaport, S., Melia, F.: *Astrophys. J.* **535**, 798 (2000). arXiv:astro-ph/9905371. doi:10.1086/308860
- Neilsen, J., Remillard, R.A., Lee, J.C.: *Astrophys. J.* **737**, 69 (2011). 1106.0298. doi:10.1088/0004-637X/737/2/69
- Neilsen, J., Remillard, R.A., Lee, J.C.: *Astrophys. J.* **750**, 71 (2012). 1203.0301. doi:10.1088/0004-637X/750/1/71
- Press, W.H., Teukolsky, S.A., Vetterling, W.T., Flannery, B.P.: *Numerical Recipes 3rd Edition: The Art of Scientific Computing*, 3rd edn. Cambridge University Press, New York, NY, USA (2007)
- Pringle, J.E., Rees, M.J., Pacholczyk, A.G.: *Astron. Astrophys.* **29**, 179 (1973)
- Regev, O., Buchler, J.R.: *Astrophys. J.* **250**, 769 (1981). doi:10.1086/159426
- Shakura, N.I., Sunyaev, R.A.: *Mon. Not. R. Astron. Soc.* **175**, 613 (1976)
- Shilnikov, A., Kolomiets, M.: *I. J. Bifurcation and Chaos* **18**(8), 2141 (2008)
- Strogatz, S.H.: *Nonlinear Dynamics And Chaos: With Applications To Physics, Biology, Chemistry, And Engineering (studies in Nonlinearity)*, 1st edn. Studies in nonlinearity. Perseus Books Group, New York City (1994)
- Taam, R.E., Lin, D.N.C.: *Astrophys. J.* **287**, 761 (1984). doi:10.1086/162734
- Taam, R.E., Chen, X., Swank, J.H.: *Astrophys. J. Lett.* **485**, 83 (1997). doi:10.1086/310812
- Watarai, K.-y., Mineshige, S.: *Astrophys. J.* **596**, 421 (2003). astro-ph/0306548. doi:10.1086/377576

Appendix I - Derivation of FhN equations

Consider the two equations of the general system given of Eq. (4) written using the variables $\tilde{x}(\tilde{t})$ and $\tilde{y}(\tilde{t})$:

$$\begin{aligned}\frac{d\tilde{x}}{d\tilde{t}} &= \frac{1}{A}[-a_1\tilde{x}^3 + a_3\tilde{x} - b_1\tilde{y}] \\ \frac{d\tilde{y}}{d\tilde{t}} &= a_6\tilde{x} - b_2\tilde{y} + a_7\end{aligned}$$

and transform it by means of the following change of variables $x = (a_6/b_2)\tilde{x}$, $y = \tilde{y} - (a_7/b_2)$, and $t = b_2\tilde{t}$.

After some simple calculations one obtains:

$$\begin{aligned}\frac{dx}{dt} &= -\frac{a_1b_2}{Aa_6^2}x^3 + \frac{a_3}{Ab_2}x - \frac{a_6b_1}{Ab_2^2}y - \frac{a_6a_7b_1}{Ab_2^3} \\ \frac{dy}{dt} &= x - y\end{aligned}$$

and introducing the following coefficients

$$\begin{aligned}\rho &= \frac{a_1b_2}{Aa_6^2} \\ \chi &= \frac{a_3}{Ab_2} \\ \gamma &= \frac{a_6b_1}{Ab_2^2} \\ J &= \frac{a_6a_7b_1}{Ab_2^3}\end{aligned}$$

it becomes the same system of Eq. (6).

Appendix II - Invariant translated equations

Eqs.(6) are written in a particular simple form having a rather small number of parameters (three internal parameters and an external one). In this approach, however, the physical meaning of the parameter would not result always clear: for instance the external term J , that we related with the mass accretion rate, gives a negative contribution to the x derivative in the former of Eqs.(6), and this can appear to be unphysical.

One has to consider that the shape of Eqs.(6) solutions is invariant under a translation along the first degree nullcline. Shifting both x and y of the same quantity δ , we can define the new variables $\xi = x + \delta$ and $\eta = y + \delta$, whose time derivatives are obviously equal to those of x and y , respectively. Eqs.(6) transform into the more general ones:

$$\begin{aligned}\frac{d\xi}{dt} &= -\rho\xi^3 + \chi\xi - \gamma\eta + 3\rho\delta(\xi^2 - \delta\xi) + [G(\delta) - J] \\ \frac{d\eta}{dt} &= \xi - \eta\end{aligned}$$

where

$$G(\delta) = 3\rho\delta^3 - \chi\delta + \gamma\delta \quad .$$

It is rather simple to verify that the term in square brackets for a δ value large enough can obtain a positive value, as expected. Solutions of this system differ from those of the original Eqs.(6) only for an additive constant, thus the quantities $\xi - \delta$ and $\eta - \delta$ are invariant. It is clear that only the case $\delta = 0$, without the quadratic term, is more suitable for the study of nullcline properties, and for this reason we considered it in our work.

Appendix III - Stability and limit cycle conditions

Here we present a synthetic description of main results concerning the stability of equilibrium points and the conditions to have a limit cycle within a limited region surrounding them. A complete mathematical description will be given in a separate paper (Ardito et al., in prepatation). The equilibrium points are the solutions of the cubic Eq. (9)

$$\varphi(x) = x^3 + \frac{\gamma - \chi}{\rho} x + \frac{J}{\rho} = 0$$

Three cases must be considered: *i*) $\chi < \gamma + 3(\rho J^2/4)^{1/3}$, there is only a unique real solution $x_* < 0$ and therefore only one equilibrium point (x_*, y_*) exists;

ii) $\chi = \gamma + 3(\rho J^2/4)^{1/3}$, there are a negative solution $x_* < -\sqrt{(\chi - \gamma)/(3\rho)}$ and a double positive solution $x_0 = \sqrt{(\chi - \gamma)/(3\rho)}$, the system has two equilibrium points;

iii) $\chi > \gamma + 3(\rho J^2/4)^{1/3}$, there are three real solutions x_*, x_1, x_2 , with $x_* < -\sqrt{(\chi - \gamma)/(3\rho)} < x_1 < \sqrt{(\chi - \gamma)/(3\rho)} < x_2$, and therefore the system has three equilibrium points.

Considering that x_* is the unique negative solution of the equation $\varphi(x) = 0$, in the following we will use x_* as parameter instead of J .

For the study of the stability it is more convenient to define the two new variables:

$$\begin{aligned} u &= x - x_* \\ v &= (y - y_*) - (x - x_*)/\gamma \end{aligned}$$

and the system of differential equation becomes:

$$\begin{aligned} du/dt &= \gamma[f(u) - v] \\ dv/dt &= g(u) \end{aligned}$$

where

$$f(u) = -(\rho/\gamma)u[u^2 + 3x_*u + 3x_*^2 + (1/\rho) - (\chi/\gamma)]$$

and

$$g(u) = (\rho/\gamma)u[u^2 + 3x_*u + 3x_*^2 + (\gamma/\rho) - (\chi/\gamma)] ,$$

with $\chi, \rho, \gamma > 0$, $x_* < 0$, and $(\chi/\rho) < (\gamma/\rho) + x_*^2$.

The previous conditions are now written as:

i') for $0 < \chi/\rho < \gamma/\rho + (3/4)x_*^2$ there is only an equilibrium point at the origin O in the (u, v) space;

ii') for $\chi/\rho = \gamma/\rho + (3/4)x_*^2$ there are two equilibrium points, one at the origin O and the other at $E_0 = (-(3/2)x_*, -(3/2)(1 - 1/\gamma)x_*)$ in the (u, v) space;

iii') $\gamma/\rho + (3/4)x_*^2 < \chi/\rho < \gamma/\rho + x_*^2$ there are three equilibrium points $O, E_1 = (u_1, v_1), E_2 = (u_2, v_2)$, where

$$u_{1,2} = -(3/2)x_* \mp \sqrt{(\chi/\rho) - (\gamma/\rho) - (3/4)x_*^2}$$

$$v_{1,2} = (1 - 1/\gamma)u_{1,2}$$

In the case $\gamma > 1$, that is the interesting one for us, from the linear analysis (Hale and Kocak 1991) one obtains the following results:

i')

for $\chi/\rho < 1/\rho + 3x_*^2$, O is locally asymptotically stable;

for $\chi/\rho = 1/\rho + 3x_*^2$, O is linearly stable;

for $\chi/\rho > 1/\rho + 3x_*^2$, O is unstable;

ii') E_0 is always unstable, whereas for O we obtain the following conditions:

for $0 < 1/\gamma < 1 - (9\rho/4\gamma)x_*^2$, O is unstable;

for $0 < 1/\gamma = 1 - (9\rho/4\gamma)x_*^2$, O is linearly stable;

for $1/\gamma > 1 - (9\rho/4\gamma)x_*^2$, O is locally asymptotically stable;

iii') E_1 is always unstable, E_2 is locally asymptotically stable, whereas for O we obtain the following:

for $\chi/\rho > \max(\rho/\gamma + (3/4)x_*^2, (1/\rho) + 3x_*^2)$, O is unstable;

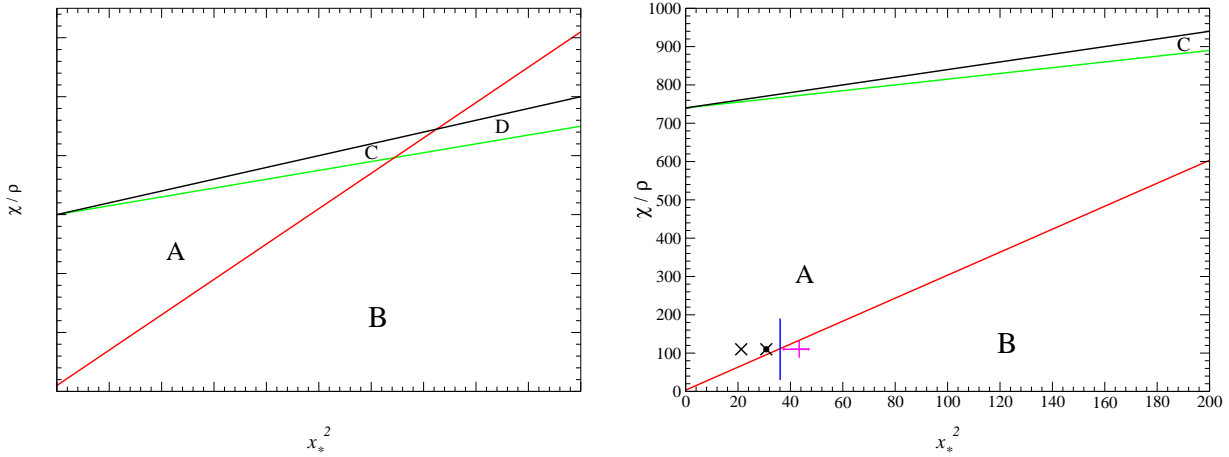


Fig. 14 Stability plot in the plane (χ/ρ) vs x_*^2 , for the FhN-A model. Upper panel: black, green and red lines correspond to equations (A1), (A2) and (A3), respectively, which define the four regions A, B, C and D in which solutions have different stability, as explained in the text. Units are arbitrary.

Lower panel: the same plot for the model FhN-A describing the ρ class bursts: the cross with a circle marks the point corresponding to the numerical solution for the F7 series ($J = 1100$, see Sect. 3.1) and the simple cross the solution for the A8b series ($J = 900$); the blue line corresponds to the equilibrium point for $J = 1190$, for which the transition to stability occurs; the magenta line is the interval where is obtained the solution plotted in Fig. 13.

for $\chi/\rho = (1/\rho) + 3x_*^2$, O is linearly stable;

for $\gamma/\rho + (3/4)x_*^2 < \chi/\rho < (1/\rho) + 3x_*^2$, O is locally asymptotically stable.

It is useful to consider the space of the two parameters χ/ρ and x_*^2 , represented in the two panels of Fig. A1. Here the black, green and red lines are given by the respective equations:

$$(\chi/\rho) = (\gamma/\rho) + x_*^2 \quad (\text{A1})$$

$$(\chi/\rho) = (\gamma/\rho) + \frac{3}{4}x_*^2 \quad (\text{A2})$$

and

$$(\chi/\rho) = (1/\rho) + 3x_*^2 \quad (\text{A3})$$

where the first equality is the upper limit of acceptable values of χ/ρ .

We obtain thus four regions, marked by the letters A, B, C, and D where the system stability is:

- region A: there is only one unstable equilibrium point;
- region B: there is only one equilibrium point which has asymptotic local stability;
- region C: there are three equilibrium points, two of which are unstable and the third has an asymptotic local stability;
- region D: there are three equilibrium points, one is unstable and the other two have asymptotic local stability.

The lower panel in Fig. A1 shows the same plane for the numerical solutions we obtained for the A8b and F7 series. The corresponding points in this plane are indicated by a cross: they lie in region A, and the latter is close to the boundary line with stable region B. A small change in the value of J can move the equilibrium point across the red line into the stable region with a disappearance of the bursting. The vertical blue line marks the value of x_*^2 for $J=1190$, for which we have the transition to a stable solution.

In the third case of i' , that corresponds to the region A in Fig. A1, we have $u g(u) > 0$, $\forall u \neq 0$ and $f(u) = -(\rho/\gamma)u(u - \tilde{u}_1)(u - \tilde{u}_2)$, with $\tilde{u}_{1,2} = -(3/2)x_* \mp \sqrt{(\chi/\rho) - (1/\rho) - (3/4)x_*^2}$.

Taking $\forall \theta \in [0, \sqrt{\rho((3/4)x_*^2 + (\gamma/\rho) - (\chi/\rho))}]$, we can consider the family of Lyapunov functions (Farkas 1994):

$$V_\theta(u, v) = \frac{1}{\gamma} \int_0^u g(s) ds + \frac{\theta}{\gamma} uv + \frac{v^2}{2} \quad .$$

Let us observe that $\forall c > 0$ the equation $V_\theta(u, v) = c$ defines a simple closed curve that is the boundary of the domain

$$\mathcal{D}(\theta, c) = \{(u, v) \in \mathbf{R}^2 | V_\theta(u, v) < c\} \quad ,$$

which includes the equilibrium point O .

It is possible to demonstrate that for $\theta = 0$ and for every initial point $(\bar{u}, \bar{v}) \neq (0, 0)$ it exists $\bar{t} > 0$ such that for $t > \bar{t}$ we have that $(u(t, \bar{u}), v(t, \bar{v}))$ lies outside the domain $\mathcal{D}(0, c_0)$ where

$$c_0 = \frac{1}{\gamma} \int_0^{\tilde{u}_1} g(s) ds \quad .$$

Moreover, because the derivative of $V_\theta(u, v)$ tends to $-\infty$ for $\|(u, v)\| \rightarrow \infty$, one has that at least one $c(\theta) > 0$ exists such that, for $\forall c > c(\theta)$ it exists $\tilde{t} > 0$ such that for $t > \tilde{t}$ we have that $(u(t, \bar{u}), v(t, \bar{v})) \in \mathcal{D}(\theta, c)$.

Finally, for

$$\bar{c} > c_0 + (\theta/\gamma) (\max\{uv \mid (u, v) \in \overline{\mathcal{D}}(0, c_0)\}) \quad ,$$

it follows that

$$\mathcal{D}(0, c_0) \subset \mathcal{D}(\theta, \bar{c})$$

that implies the existence of at least one periodic solution.